Mon. Not. R. Astron. Soc. **000**, 1–11 (2010) Printed 1 January 2013 (MN LaTeX style file v2.2)

arXiv:1212.5268v2 [astro-ph.CO] 28 Dec 2012

The Planetary Nebulae Population in the Nuclear Regions of M31: the SAURON view

Nicola Pastorello[1⋆], Marc Sarzi[2], Michele Cappellari[3], Eric Emsellem[4,5],
Gary A. Mamon[6], Roland Bacon[5], Roger L. Davies[3], P. Tim de Zeeuw[4,7]
[1] *Centre for Astrophysics and Supercomputing, Swinburne University, Hawthorn, VIC 3122, Australia*
[2] *Centre for Astrophysics Research, University of Hertfordshire, College Lane, Hatfield, Herts, AL10 9AB, UK*
[3] *Sub-Dept of Astrophysics, Dept of Physics, University of Oxford, Denys Wilkinson Building, Keble Road, Oxford, OX1 3RH, UK*
[4] *European Southern Observatory, Karl-Schwarzschild-Str 2, 85748 Garching, Germany*
[5] *Centre de Recherche Astronomique de Lyon, 9 Avenue Charles André, 69230 Saint Genis Laval, France*
[6] *Institut d'Astrophysique de Paris (UMR 7095: CNRS & UPMC), 98 bis Bd Arago, 75014 Paris, France*
[7] *Sterrewacht Leiden, Universiteit Leiden, Postbus 9513, 2300 RA Leiden, The Netherlands*

1 January 2013

ABSTRACT

The study of extragalactic Planetary Nebulae (PNe) in the optical regions of galaxies, where the properties of their stellar population can be best characterised, is a promising ground to better understand the late evolution of stars across different galactic environments. Following a first study of the central regions of M32 that illustrated the power of integral-field spectroscopy (IFS) in detecting and measuring the [O III]$\lambda 5007$ emission of PNe against a strong stellar background, we turn to the very nuclear PN population of M31, within ∼80 pc of its centre. We show that PNe can also be found in the presence of emission from diffuse gas, as commonly observed in early-type galaxies and in the bulge of spirals, and further illustrate the excellent sensitivity of IFS in detecting extragalactic PNe through a comparison with narrow-band images obtained with the Hubble Space Telescope. Contrary to the case of the central regions of M32, the nuclear PNe population of M31 is only marginally consistent with the generally adopted form of the PNe luminosity function (PNLF). In particular, this is due to a lack of PNe with absolute magnitude M_{5007} brighter than -3, which would only result from a rather unfortunate draw from such a model PNLF. The nuclear stellar population of M31 is quite different from that of the central regions of M32, which is characterised in particular by a larger metallicity and a remarkable UV-upturn. We suggest that the observed lack of bright PNe in the nuclear regions of M31 is due to a horizontal-branch population that is more tilted toward less massive and hotter He-burning stars, so that its progeny consists mostly of UV-bright stars that fail to climb back up the asymptotic giant branch (AGB) and only of few, if any, bright PNe powered by central post-AGB stars. These results are also consistent with recent reports on a dearth of bright post-AGB stars towards the nucleus of M31, and lend further support to the idea that the metallicity of a stellar population has an impact on the way the horizontal branch is populated and to the loose anticorrelation between the strength of the UV-upturn and the specific number of PNe that is observed in early-type galaxies. Finally, our investigation also serves to stress the importance of considering the same spatial scales when comparing the PNe population of galaxies with the properties of their stellar populations.

Key words: galaxies: elliptical and lenticular – galaxies: stellar content – galaxies: individual: M31 – ISM: planetary nebulae: general – stars: AGB and post-AGB

1 INTRODUCTION

Planetary Nebulae (PNe) in external galaxies are mostly regarded either as tracers of the gravitational potential (e.g., Romanowsky et al. 2003; Douglas et al. 2007) or as indicators for the distance of their galactic hosts (e.g., Ciardullo et al. 1989; Jacoby, Ciardullo, & Ford 1990; Jacoby et al. 1992), with the latter advantage owing to the nearly universal – though not fully understood – shape of the PNe luminosity function (PNLF, generally in the [O III]$\lambda 5007$ emission). Yet extra-galactic PNe

---

⋆ E-mail: npastorello@swin.edu.au

© 2010 RAS

can also be used as probes of their parent stellar population (e.g., Richer, Stasińka, & McCall 1999; Jacoby & Ciardullo 1999; Dopita et al. 1997) and understanding in particular the origin of the PNLF is a puzzle that, once solved, promises to reveal new clues on the late stages of stellar evolution and on the formation of PNe themselves (see, e.g., Ciardullo 2006).

PNe originate from horizontal-branch (HB) stars that climb back up the asymptotic giant branch (AGB) at the end of their helium-burning phase, after which these stars leave the AGB and quickly cross the Hertzprung-Russell diagram on their way towards the cooling track of white dwarves (WD). For a population with a given age and metallicity, HB stars have nearly the same helium core mass ($\sim 0.5\,M_{\odot}$) but a range of hydrogen shell mass ($\sim 0.001 - 0.3\,M_{\odot}$), with the reddest stars having also the largest H-shells and originating from the most massive main-sequence progenitors. Only HB stars with a considerable H-shell ascend toward the AGB and eventually lead to the formation of a PN (being known at this point as post-AGB or early post-AGB stars depending on their UV brightness), whereas the bluest HB stars with little envelope mass head straight toward the WD cooling curve by evolving first to higher luminosities and effective temperatures (the so-called AGB-manqué phase, see Greggio & Renzini 1999).

According to this simple picture, galaxies with on-going star formation should show brighter PNe than quiescent systems where massive stars have long disappeared (e.g., Marigo et al. 2004 show that the most luminous PNe arise from 1 Gyr old 2.5 $M_{\odot}$ stars), but in fact the PNLF of young and old galaxies are relatively similar. In particular, all extra-galactic PNe surveys indicate a common and bright cut-off for the PNLF, which led Ciardullo et al. (2005) to suggest a binary evolution for the progenitors of the brightest PNe that would be common to different kind of galaxies. Alternatively, a similarly bright PNLF cutoff in elliptical galaxies might be explained by minor mergers mixing in 1 Gyr old stars with the much older stellar population of these galaxies (Mamon, Dekel, & Stoehr 2005). If galaxies seem to invariably host very bright PNe, their specific content of PNe - that is the number of PNe normalised by a galaxy bolometric luminosity - appears to vary with the metallicity of the stellar population. More specifically, Buzzoni, Arnaboldi, & Corradi (2006) found that more metal-rich galaxies show comparably fewer PNe, which also corresponds to larger far-UV fluxes. Interestingly, this may indicate that, at a given mean stellar age, a larger metallicity would bias the HB population towards fewer stars with a massive H-shell capable of leading to the formation of PNe. On the other side, a larger fraction of blue HB stars will instead contribute to the overall far-UV flux of their host galaxy (i.e. the so-called UV-upturn, Burstein et al. 1988) as they follow their AGB-manqué evolution. This trend is not completely unexpected given that the mass of the H-shell around HB stars depends on the amount of mass they have lost on the red-giant branch and that in turn the mass-loss rate efficiency η should increase with stellar metallicity (Greggio & Renzini 1990). Yet, it must be borne in mind that η could also follow an increase in the abundance of Helium that may also come with a larger stellar metallicity.

Within this context, we note that whereas our knowledge of both the shape and normalisation of the PNLF comes chiefly from the peripheral PN populations of galaxies, measurements of both the stellar metallicity and the UV spectral shape of galaxies pertain to their optical regions. Indeed, with ground-based narrow-band imaging or slitless spectroscopy - the most common techniques employed to find extragalactic PNe - is is difficult to detect PNe against a strong stellar background, whereas measuring the strength of stellar absorption lines or imaging the far-UV flux of galactic halos is prohibitively expensive in terms of telescope time. Such a dramatic spatial inconsistency needs to be resolved to understand the link between PNe and the properties of their parent stellar populations, in particular if we consider that such a connection may already not be entirely within our grasp, as suggested by the Hubble Space Telescope (*HST*) observations of M32 obtained by Brown et al. (2008) who uncovered a dearth of UV-bright stars compared to what expected from stellar evolutionary models.

In our investigation of the compact elliptical M32 (Sarzi et al. 2011, hereafter Paper I) we have demonstrated how integral-field spectroscopy can overcome the previous limitations and detect PNe in the central regions of galaxies. In fact, with `SAURON` data taken with just two 10-minute pointings we could double the number of known PNe within the effective radius of M32 and detect PNe five times fainter than previously found in narrow-band images that collected nearly the same number of photons. Here we will turn our attention to the nuclear regions of M31, using `SAURON` observations of similar depth and spatial coverage, and motivated by the known differences between the stellar metallicity and UV colours of M31 and M32 (e.g., Burstein et al. 1988).

This paper is structured as follows. In §2, we briefly review the acquisition and the reduction of the `SAURON` data for M31. In §3, we detail our method for identifying PNe and measuring their [O III]λ5007 flux, accounting also for the presence of diffuse ionised-gas emission in M31 and comparing our PN detections and flux measurements with the ones obtained from *HST* narrow-band imaging. In §4, we assess whether our data are consistent with the generally adopted shape for the PNLF, finding evidence for a dearth of bright PNe in the nuclear regions of M31, which we then discuss in §5 in the context of the stellar population properties of this and other galaxies. Finally, in §6 we draw our conclusions.

Throughout this paper we assume a distance of 791 kpc for M31, taken to be equal to that to M32 based on the surface-brightness fluctuation measurements of Tonry et al. (2001).

2 OBSERVATIONS AND DATA REDUCTIONS

M31 (NGC 224) was one of the special objects that were observed over the course of the `SAURON` representative survey (de Zeeuw et al. 2002). Its central regions were observed with two 1800s slightly offset pointings and using the low-resolution mode of `SAURON`, which gives a $33\farcs0 \times 44\farcs0$ field-of-view fully sampled by $0\farcs94 \times 0\farcs94$ square lenses (for more details on the instrument see Bacon et al. 2001a). At the assumed distance of 791 kpc such an field corresponds to a circular area 76 pc in radius. The data from each pointing were reduced similarly to the data obtained for the objects of the main `SAURON` sample (see Emsellem et al. 2004; Falcón-Barroso et al. 2006), and the resulting datacubes were merged and resampled in $0\farcs8 \times 0\farcs8$ spatial elements each corresponding to spectra covering the wavelength range between 4830Å and 5330Å with a final spectral resolution of 4.2Å (FWHM, for a $\sigma_{\rm res} = 108{\rm km\ s^{-1}}$). The only differences with the data used in the papers of the `SAURON` project are that here we did not perform any Voronoi spatial binning (Cappellari & Copin 2003), to avoid swamping the signal of the weaker PNe against an increased stellar background, and that we re-adjusted the absolute flux calibration of the `SAURON` cube using data obtained with *HST*.

In particular, we have used archival Wide-Field Planetary Camera (WFPC2) narrow-band images obtained in the F502N passband, since this filter falls entirely within the wavelength range

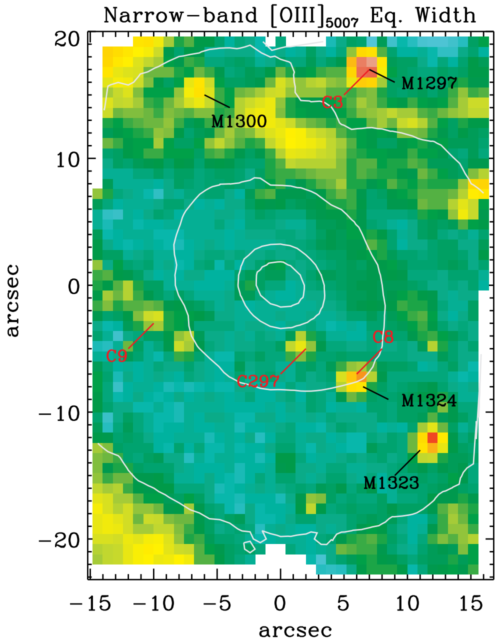

Figure 1. Map of the equivalent width (EW) of the estimated [O III]λ5007 flux from narrow-band imaging based on the SAURON data. The flux in the [O III] region is measured through a 2.5Å-wide spectral window centred on the expected position of [O III] given the systemic velocity of $V_{\rm sys} = -300\,{\rm km\,s^{-1}}$ for M31, whereas the flux of the stellar continuum is computed using the mean spectral energy density across the entire spectrum times the same 2.5Å wavelength interval. The difference between these two flux measurements gives an estimate of the [O III] flux, which once divided by the mean spectral energy density in the stellar continuum leads to the mapped EW values. The map shows both the presence of diffuse gas and of isolated patches of [O III] emission that could originate from the unresolved [O III] emission of PNe, more or less embedded in the diffuse gas component. Several of the brightest sources in this figures were already identified as PNe by Ciardullo et al. (1989, red labels) and Merrett et al. (2006, black labels). In this and subsequent SAURON maps of M31, north is up an east is to the left.

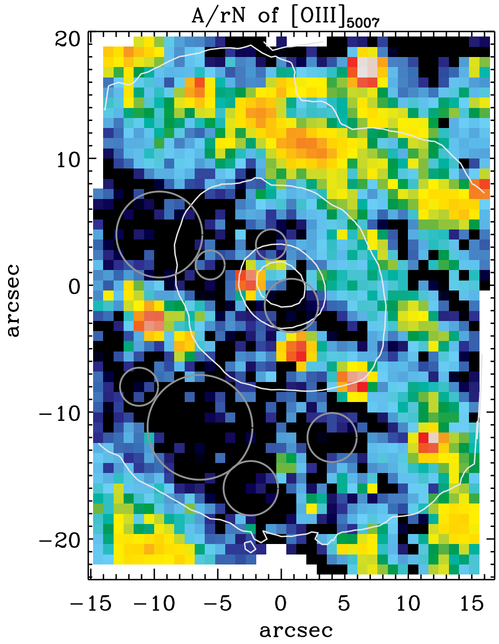

Figure 2. Map of the values of the A/rN ratio for the [O III]λ5007 lines following our analysis of the SAURON spectra. The A/rN values are shown in a logarithmic scale (from values of 1 to 64) and dark-blue bins correspond to regions where $A/rN < 4$ and the [O III] lines are not formally detected. The grey circles in these regions show the aperture over which the SAURON spectra were added up to obtain high-quality spectra that formed the basis for our description of the stellar continuum in our data. Both the extent of the diffuse ionised-gas emission and the presence of a number of [O III] unresolved sources consistent with PNe can be better appreciated here compared to Fig. 1. An additional known PN near the centre M31 (Bacon et al. 2001b) is now also revealed.

of our SAURON data and because the typical old stellar spectrum of early-type galaxies and bulges can be considered pretty much as a flat spectral energy density source across the F502N filter. In fact, since the PHOTFLAM keyword in the *HST* images is defined as the flux density of a flat spectral source (in ${\rm erg\,s^{-1}cm^{-2}\AA^{-1}}$) that would produce a flux corresponding to one count per second, this situation allows to use the PHOTFLAM keyword to construct a flux-density profile that can be readily matched (accounting for the different pixel size) to the radial trend for the median flux density of our SAURON spectra (where such a median value is not affected by the presence of [O III] emission).

3 DATA ANALYSIS

3.1 Emission-line Measurements

In order to identify the PNe in the nuclear regions of M31 and measure their flux in the [O III]λ5007 line, we first need to separate as accurately as possible the stellar and nebular contribution to each of the SAURON spectra, and then to further disantangle the emission due to PNe from the one arising from diffuse gas.

Extended ionised-gas emission is common in early-type galaxies and in the bulges of disc galaxies (Sarzi et al. 2006; Falcón-Barroso et al. 2006). A first [O III] narrow-band image made from the SAURON data (Fig. 1, see caption for details) indeed reveals prominent lanes of diffuse emission, as well as a number of compact sources of [O III] emission, some of which were already recognised as PNe by Ciardullo et al. (1989) and Merrett et al. (2006).

In principle, the PNe and diffuse ionised-gas emission have sufficiently distinct characteristics to produce complicated line profiles where both components occur, such that properly extracting the flux of a PN surrounded by diffuse emission may require to separate the relative contribution of these components directly in the spectra (for instance through a double-Gaussian fit). In fact, across a given region where a putative PN would spread its nebular flux according to the telescope and seeing point-spread function (PSF), the PNe emission lines should be spectrally unresolved in our spectra (PNe have an intrinsic line profile with a velocity dispersion of only of few tens of ${\rm km\,s^{-1}}$, much smaller than our instrumental resolution), falling always at the position corresponding to the velocity of the PN and with a strength - or peak spectral density amplitude - that varies between different spatial bins according to the shape of the PSF (e.g. a bi-dimensional Gaussian). The putative PN spectrum should also be always characterised by the same [O III]/Hβ line ratio. On the other hand, the diffuse ionised-gas emission could, in principle, come with different kinematics, strength and line-ratios across the entire region where the PN emission is found.

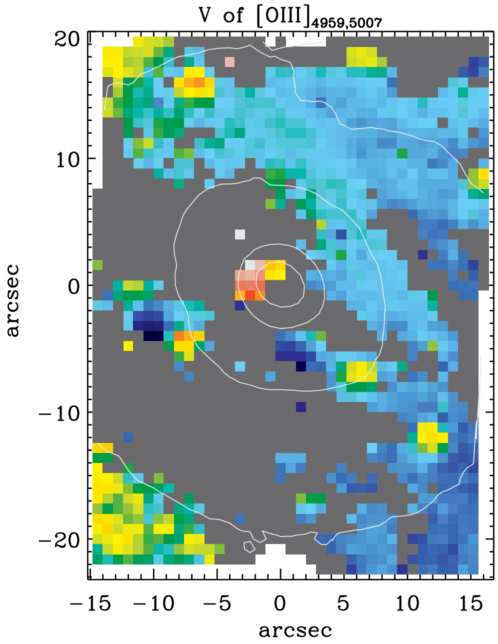

Figure 3. Velocity of the [O III]$\lambda\lambda4959, 5007$ lines detected across the nuclear regions of M31, from values of -300 to 300 $\mathrm{km\ s^{-1}}$ relative to the systemic velocity of M31. Rather coherent motions are observed along the extended lanes of diffuse ionised-gas emission, whereas regions dominated by the [O III] emission of known or putative PNe display similarly distinct velocity values. Grey areas in this and subsequent figures correspond to regions with no detected [O III] emission.

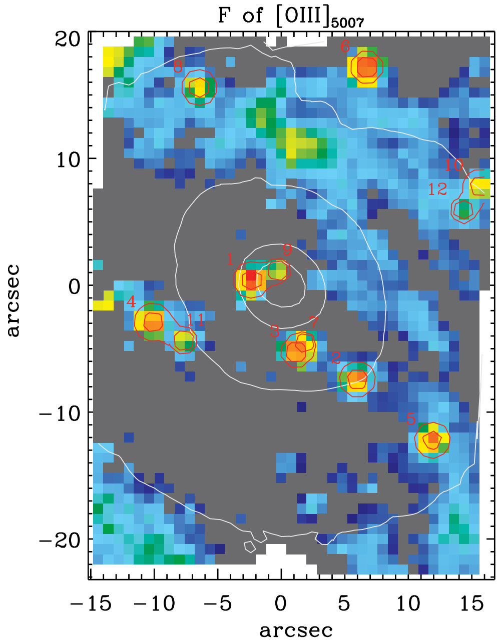

Figure 4. Map of the flux of the [O III]$\lambda5007$ emission from M31, in logarithmic scale from values of 0.5 to 50 $\times$ $10^{-16}\mathrm{erg\,s^{-1}cm^{-2}arcsec^{-2}}$, showing both the diffuse ionised-gas component and each of the PNe considered in this paper. PNe sources are labelled and delineated by red contours corresponding to our best-fitting Gaussian model to their observed flux distribution, which is used to compute their total [O III] flux F_{5007} and corresponding detection limit (see text). The inner contour around each PNe shows the half-peak flux level of the Gaussian model, thus corresponding to a circle a FWHM in diameter, whereas the second contour shows the region containing 90% of the flux of the model around each PN, or of both the Gaussians models in the case of blended PNe sources.

In practice, however, we do not expect to observe dramatic variations in the properties of the diffuse gas where the light of a given PN falls, either because such fluctuations are not likely to occur across the physical scale that correspond to a seeing disc (that is, $\sim$ 14 pc for a $\sigma_{\rm PSF} = 0\farcs61$ - see §3.2 for how this is derived) or since they will be considerably levelled by the PSF itself anyway (for instance, see Fig. 3 below for an illustration of how smooth the motion of the diffuse component is). Furthermore, the velocity of the PNe in the nuclear regions of M31 is unlikely to differ from that of the diffuse ionised-gas by more than a few 100 $\mathrm{km\ s^{-1}}$ given the modest value for the stellar velocity dispersion ($\sim$160 $\mathrm{km\ s^{-1}}$; Saglia et al. 2010) and that both gas and stars rotate relatively slowly (at $\sim$ 50 and 100 $\mathrm{km\ s^{-1}}$, respectively). This means that the observed line profiles should not be exceedingly complicated in the presence of both PN and diffuse gas components (given the limited spectra resolution of our data), remaining in particular in the regime where a single Gaussian profile estimates sufficiently well the *total* nebular flux in our spectra[1] and thus allowing us to subsequently discern the presence of PNe using only a spatial analysis of the [O III] flux distribution.

For these reasons we proceeded to extract the ionised-gas flux values in our spectra by adopting the fitting method of Sarzi et al. (2006), whereby a set of stellar templates and Gaussian emission lines are fitted simultaneously to the spectra[2], while adopting the approach of Sarzi et al. (2010) to further improve the match to the stellar continuum and ensure that the ionised-gas emission is extracted from the subtraction of a physically motivated stellar model.

As a first result of this procedure, Fig. 2 shows the map of the ratio between the amplitude A of the best-fitting Gaussian to the [O III]$\lambda5007$ line and the noise level rN in the residuals of the overall fit. The value of the A/rN ratio relates to the accuracy with which the flux, position and width of a single emission line can be estimated, with tests indicating a formal detection for $A/rN > 4$ (Sarzi et al. 2006). Dark blue colours in Fig. 2 show regions with no detected [O III] emission (hereafter shown in grey) and where high-quality SAURON aperture spectra were extracted and subsequently converted into stellar templates in order to improve our spectral fit (Sarzi et al. 2010).

Compared to Fig. 1, the known PNe in the nuclear regions of M31 show up with a greater contrast as unresolved sources in the A/rN of Fig. 2, which further reveals the extent of the diffuse ionised-gas emission and the presence of the central PN already

---

[1] Simple tests show that a single Gaussian fit to double-Gaussian profiles allow to estimate to total flux with less than 10% uncertainty as long as the two Gaussian components are separated by less than 3 times their common dispersion. This is irrespective of the relative strength of the two Gaussians but assumes similar values for their dispersion, which is justified for our case study where both the PNe and the diffuse gas emission are characterised by intrinsic profiles that are hardly resolved.

[2] In practice this is achieved by using the IDL code GANDALF (available at `http://star-www.herts.ac.uk/~sarzi`) and the stellar kinematics extracted with the pixel-fitting IDL code pPXF (Cappellari & Emsellem 2004, `http://www-astro.ox.ac.uk/~mxc/idl`)

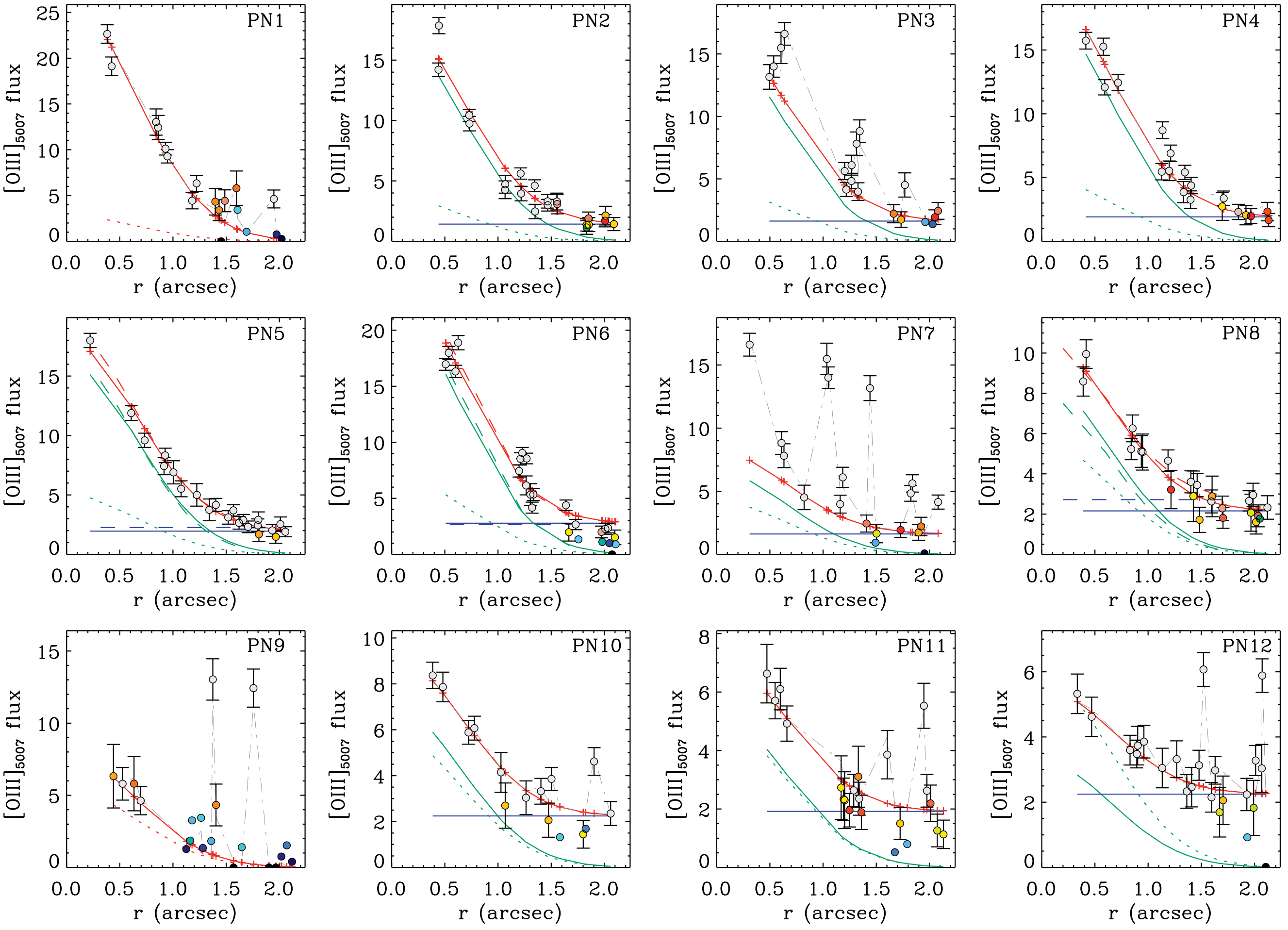

Figure 5. Radial profiles for the [O III]λ5007 line flux (in $10^{-16}\mathrm{erg\,s^{-1}cm^{-2}arcsec^{-2}}$) observed around the PNe shown in Fig. 4, along with the corresponding best-fitting model for such a flux distribution (red lines, models are resampled in the `SAURON` $0\farcs8 \times 0\farcs8$ bins), which generally comprises a Gaussian component representing the unresolved emission from the PN (green lines) and a constant background level of diffuse ionised-gas emission (blue lines). Radial distances are computed from the centre of the Gaussian models and the data points are colour coded according to the value of the A/rN ratio. Colours change from blue to red for increasing values of A/rN till they saturate to white for $A/rN > 8$. Green corresponds to the detection threshold of $A/rN = 4$, above which the data points are also plotted together with error bars for the [O III] flux. The dotted coloured lines show the Gaussian model for the faintest PN flux that we could detect (see text). For PNe 12 this limit exceeds the total measured [O III] flux, and should thus be formally regarded as marginal case. PNe 1 and 9, 3 and 7, 4 and 11 as well as 10 and 12 have been modeled simultaneously, and in their corresponding panel the contribution of their companion PN can be appreciated by following the dot-dashed grey line. Finally, the dashed coloured lines for PNe 5, 6 and 8 show the models obtained through a simultaneous spectral and spatial fitting of the [O III] emission (see text).

detected with integral-field data by Bacon et al. (2001b) A few additional unresolved sources could be present in Fig. 2, for instance around 8″ east of the nucleus and next to PN C9 of Ciardullo et al. (1989) or next the western edge of the `SAURON` field-of-view and around 8″ north of the nucleus.

The kinematics of the [O III] lines provides more elements to judge whether a given patch of [O III] is likely to originate from a PN, since PNe are expected to generally move with a different velocity than the gas clouds responsible for the diffuse [O III] emission that may be found along the same line of sight. Fig 3 shows indeed that where the known PNe dominate the nebular emission, the [O III] kinematics appears quite coherent and at the same time significantly different from that of the surrounding diffuse component when this is present. This seems to be the case also for the two aforementioned putative sources, with the possible addition of few more regions.

3.2 PNe Detection and Flux Measurements

In order to measure the total [O III] emission of the known PNe in the nuclear regions of M31 and assess more precisely the presence of additional sources, we proceeded to fit the [O III] flux distribution around any putative PNe with a bi-dimensional Gaussian profile meant to represent the PSF, like already detailed in Paper I (including the possibility to match blended sources). Furthermore, we now also allow for a constant background level to account for the diffuse ionised-gas emission. During each of these fits, we adjusted the position and amplitude of the Gaussian models as well as the level of the background, whereas the full-width at half maximum (FWHM) of the PSF was optimized over the whole set of sources that were eventually deemed detected. This turned out to have a value of $1\farcs44$, for a $\sigma_{\rm PSF} = 0\farcs61$. Considering a constant level for the background diffuse emission certainly represents a simple approximation and yet, despite it being meant initially only as a

Table 1. Basic Properties of the PNe in the Optical Regions of M31

ID (1)	x-off (2)	y-off (3)	F_{5007} (4)	δF_{5007} (5)	$F_{5007,\mathrm{lim}}$ (6)	$F_{5007,\mathrm{spec}}$ (7)	$F_{5007,HST}$ (8)	V_{PN} (9)	$V_\star$ (10)	$\sigma_\star$ (11)	[O III]/Hβ (12)
1	-2.35	0.42	80.3	3.1	8.6	—	66.7	262.3	57.3	120.4	> 15.1
2	6.00	-7.39	52.7	2.8	11.3	—	37.6	44.4	-24.3	153.1	8.0
3	1.17	-5.28	47.3	10.9	12.9	—	64.6	-183.4	0.5	140.3	> 12.7
4	-10.10	-2.91	55.1	2.4	15.2	—	47.1	-214.1	21.8	144.5	17.2
5	11.91	-12.20	49.3	1.5	15.5	46.4	—	61.2	-31.2	155.1	7.4
6	6.74	17.18	66.6	4.7	22.1	66.4	—	13.1	10.6	176.0	11.5
7	1.81	-4.57	20.1	10.1	12.9	—	11.9	-127.1	-7.8	144.2	> 10.2
8	-6.45	15.59	26.1	1.9	17.2	22.1	19.7	110.5	18.3	139.4	7.4
9	-0.27	1.15	24.0	5.3	16.7	—	25.4	85.1	82.6	167.9	> 2.8
10	15.65	7.83	21.5	1.4	17.8	—	17.3	25.1	-16.1	160.4	5.2
11	-7.68	-4.35	16.1	2.8	15.2	—	19.9	108.1	6.7	138.7	> 7.9
12	14.36	5.93	9.9	1.4	17.8	—	9.7	-50.6	-9.9	157.3	5.0

Notes: (1) PN ID. (2)–(3) R.A. and Declination offset position, in arcseconds, from the centre of M31. (4)–(6) Total [O III]$\lambda 5007$ flux F_{5007} in $10^{-16}\mathrm{erg\,s^{-1}cm^{-2}}$, with associated formal error and detection limit. (7)–(8) Same as Col. (4) but now for F_{5007} values measured through a simultaneous spectral and spatial fit of the SAURON data, and from WFPC2 narrow-band images in the F502N filter. (9) Velocity of the PN, in $\mathrm{km\,s^{-1}}$ and relative to the systemic velocity of M31, measured in spectra extracted within a FWHM-wide aperture around the center of the best-fitting Gaussian models shown in Figs. 4 and 5. (10)–(11) Velocity and velocity dispersion of the stars along the line-of-sight pointing to the direction of the PN, measured from the same aperture spectra. (12) [O III]/Hβ ratio, again in the same spectra. An upper-limit is listed when Hβ is not detected, using an Hβ flux that would correspond to lines with the same profile as the [O III] lines and with an amplitude equal to 3 times the level of noise in the fit residuals (i.e., the detection threshold for Hβ, following Sarzi et al. 2006).

starting point for our modelling, this approach eventually turned out to work as well as more sophisticated models (see below).

In our previous analysis of M32 (Paper I), we deemed a given source that was successfully matched by our model a detected PNe if all [O III] lines are detected (i.e., $A/rN > 4$ in the present case) within at least the FWHM of the bi-dimensional Gaussian model. The presence of diffuse ionised-gas in M31 has led us to require in addition that the peak amplitude of the Gaussian model exceeds by at least a factor 3 the background level of the diffuse emission, when this is needed. Furthermore, we should make sure that where the nebular emission is dominated by our putative PNe (i.e., within a FWHM), the values for the [O III]/Hβ ratio significantly exceed the typical values observed in the filament structures in the nuclear regions of M31, which range between 1 and 3, similarly to the case of the diffuse emission of early-type galaxies (Sarzi et al. 2006).

All the PNe that we eventually detected according to these criteria are located in the map for the [O III]$\lambda 5007$ flux shown in Fig. 4. One of these sources (PN 7) was only identified following our analysis of *HST* images (see next section) and another (PN 12) represents only a marginal detection as the peak amplitude of its best-fitting bi-dimensional Gaussian is only twice the level of the background emission. Fig. 4 also nicely illustrates the relatively smooth character of the diffuse emission observed in the filamentary structures in central regions of M31, which supports our simple treatment of this component in our PNe fit as a constant background.

The quality of our fit to the [O III] flux distribution of our detected PNe sources and their immediate surroundings can also be appreciated in Fig. 5, where the radial profile for the [O III] flux of each PN is plotted together with its best-fitting Gaussian model. Fig. 5 also shows the Gaussian profile that corresponds to the limiting total PN flux that we could have measured, which is obtained by scaling down the best fitting Gaussian model until either its peak amplitude becomes less than three times the level of diffuse-gas emission (when present) or until it would induce the faintest [O III] line within a FWHM to become undetected.

For all detected PNe, Tab. 1 lists their position relative to the centre of M31, their total F_{5007} flux of the [O III] emission with its corresponding detection limit and our best estimate for their relative velocity V_{PN} and value of the [O III]/Hβ ratio (or lower-limit when Hβ is not detected). The latter two measurements are based on fits to spectra extracted within a FWHM-wide aperture, in order to maximise the emission-line signal and better isolate the kinematics and line ratio of PNe that in projection are either close to each other or appear embedded in diffuse gas. These aperture spectra were also used to measure the stellar mean velocity $V_\star$ and velocity dispersion $\sigma_\star$ along the line-of-sight pointing to the detected PNe, which can be compared to the PNe velocity V_{PN} in order to verify the PNe membership to M31. In fact, the presence of only 3 sources out of 12 with $|V_{\mathrm{PN}} - V_\star| > \sigma_\star$ is consistent with the hypothesis that, as a group, these PNe belong to M31. Tab. 1 also lists the values [O III]/Hβ ratio for our detected sources, all of which, by construction, are above 3. Finally, we note that these are the only PNe that we manage to isolate after attempting to fit the most apparent peaks of [O III] emission, and that only in one case did our fit converge on an unresolved source with a measured [O III]/Hβ < 3.

3.3 Further Flux-Measurements Tests and Cross-check with HST data

To test our purely spatial approach for isolating the PNe emission from that of the diffuse gas, we re-measured the flux of three well detected single PNe surrounded by extended emission (PNe 5, 6 and 8) by means of a somewhat more general and simultaneous spectral and spatial fit of the [O III] emission. More specifically, we re-fitted the 25 closer SAURON spectra to the centre of each of these three PNe (in a 5×5 bins aperture) by matching their [O III] lines with two Gaussian components, one for the PN emission and the other for the diffuse ionised-gas emission. Across this region, we fixed the kinematics of each set of lines, and still imposed a bi-dimensional Gaussian and constant spatial trend to the flux of the

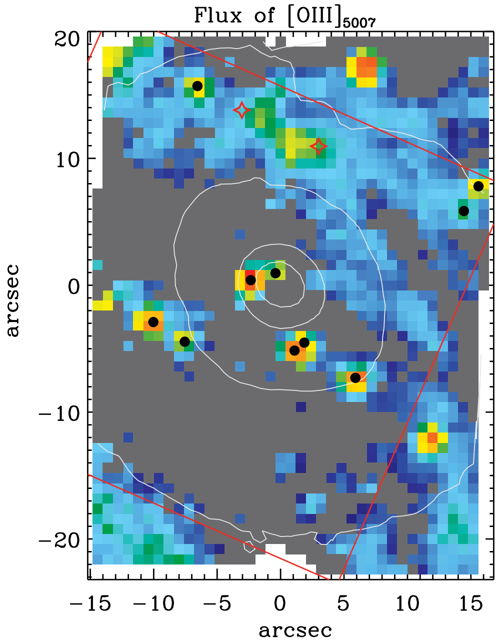

Figure 6. Map of the flux of the [O III]λ5007 emission from M31, as in Fig. 4, but now showing the PNe identified in the F502N narrow-band *HST* image (black points) and more specifically within the field-of-view of the WPFC2 planetary camera (delinated by the red lines). Each of these sources corresponds to the PNe we isolated through our analysis of the SAURON data (Fig. 4) except for PN 7, which was included in our analysis only following its identification in the HST images. The red crosses show the location of two stellar sources, most likely RGB stars.

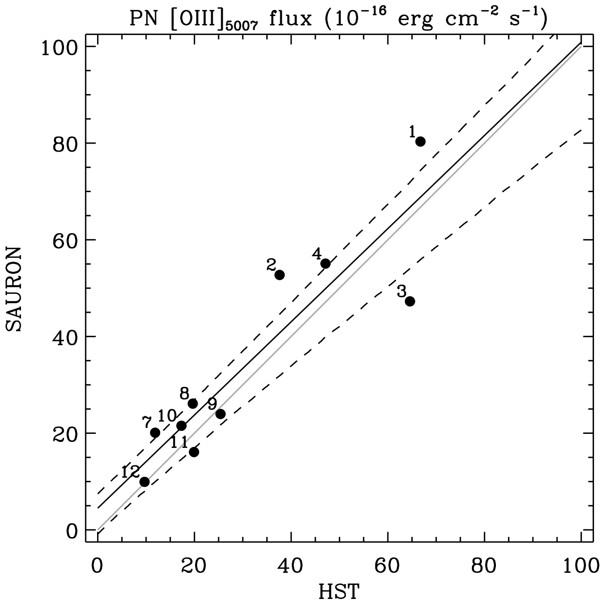

Figure 7. Comparison between the SAURON and *HST* F502N narrow-band measurements for the total [O III]λ5007 flux of the PNe found where the field-of-view of the WFPC2-PC overlapped with that of the SAURON observations. The grey line indicates the one-to-one relation, whereas the solid and dashed black lines show the best-fitting linear regression to the data and associated 68% confidence limits. The SAURON F_{5007} values follow rather closely their *HST* counterparts, with no strong evidence of any systematic offset.

Gaussian lines representing the PNe and diffuse-gas components to the observed [O III] profiles, respectively. During the fit we then optimised the centre and amplitude of the PNe profile, the level of the diffuse-gas emission, and also the position and width of the PNe and diffuse-gas lines (even though the PNe components were actually constrained to share a spectrally unresolved profile).

The resulting values for the flux of the PNe matched in this way differ by less than 15% from our earlier estimates, which is a tolerable level of discrepancy in the context of our analysis and supports the use of a simpler and purely spatial approach for extracting the flux also in the case of fainter PNe, where a spectral decomposition is more uncertain. Fig. 5 also shows the best-fitting Gaussians and constant radial profiles obtained for PNe 5, 6 and 8 through this more refined fit (dashed lines), whereas Tab. 1 lists the corresponding F_{5007} values. These flux values do not change considerably if, for instance, the background diffuse emission is treated as a plane rather than a constant level in the framework of a purely spatial analysis or if, alternatively, its amplitude is left free to vary across different bins during the previously described spectral decomposition.

The presence in the Hubble Legacy Archive (HLA) of narrow-band Hubble Space Telescope (*HST*) images for the nuclear regions of M31 provides a further opportunity to check whether we have missed any PN during our source identification and, in the process, also to check again the level of accuracy of our F_{5007} estimates. More specifically, we retrieved images taken with the Wide Field Planetary Camera 2 (WFPC2) in the F502N, F606W and F547M filters and, in this order, used them to a) initially identify possible sources of [O III] emission, b) confirm PNe candidates by detecting their Hα and [N II] emission and exclude spurious point-like sources in the F502N band (due for instance to an imperfect treatment of cosmic rays), and c) finally isolate stellar sources in the F502N images, most likely bright red-giant branch stars (RGB). We then proceeded to measure the F_{5007} flux of the PNe thus identified in the F502N image through standard aperture photometry.

Figs. 6 and 7 show the comparison between the positions and flux values of the PNe identified in the *HST* narrow-band images and through the spectral analysis of the SAURON data. Quite remarkably all the SAURON PNe sources in the field-of-view of the F502N PC image do have an *HST* counterpart (including our marginally detected PN 12), which always falls within $\sim 0''.1$ of the PN position estimated during our spatial fit to the SAURON [O III] flux values (e.g., Fig 5). The converse is also true in Fig. 6, except for PN 7 which (as already anticipated) was only recognized as part of an apparent doublet with PN 3 following the analysis of the *HST* images. Fig. 7 shows that the F_{5007} values also agree quite well, generally within 30% and with no strong evidence for a systematic offset between the *HST* and SAURON values (Tab. 1 also lists the F_{5007} values derived from the *HST* images). Our procedures for identifying PNe in the SAURON data and for measuring their total [O III] flux thus appear to be robust.

As a concluding aside, we note that our *HST* analysis revealed also the presence of two stellar sources, most likely RGB stars, in the portion of the SAURON field-of-view covered by the WFPC2 observations (Fig. 6). Incidentally, both stars fall quite close to the brightest region of diffuse nebular emission in our field, which is a coincidence that would be worth pursueing in the scientific framework concerning the nature of the stellar sources that are likely to power such diffuse gas (Sarzi et al. 2010).

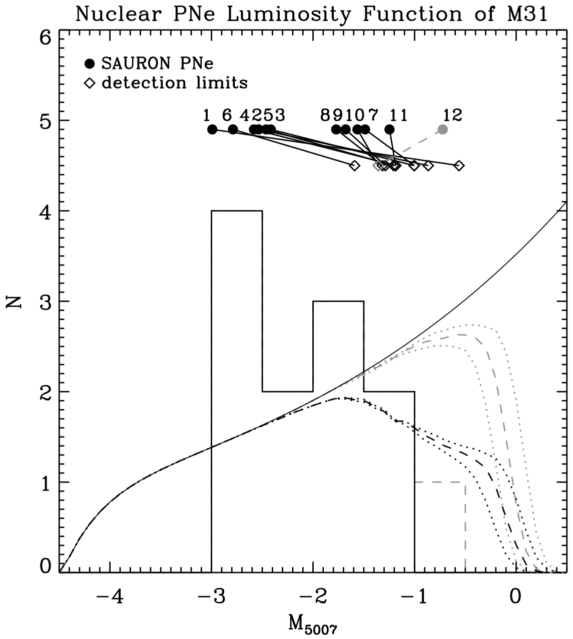

Figure 8. Luminosity function of the PNe detected by SAURON in the central 80pc of M31 (including marginal detections, dashed gray histogram), along with the theoretical form of the PNe luminosity function (solid line, from Ciardullo et al. 1989). The absolute magnitude of each PNe is shown at the top of the figure with filled circles that are plotted at an arbitrary constant ordinate and that are connected to open diamonds showing the detection limit of each source (with the marginal source PN 12 shown in grey). The dashed line shows the PNe luminosity function multiplied by the median values of the completeness function across the entire SAURON field, whereas the dotted lines indicate the range by which the expected number of detected PNe would vary depending on their exact position within the $0.''8 \times 0.''8$ SAURON bins. Such a completeness function accounts also for the presence of diffuse ionised-gas in the central regions of M31, whereas the dashed and dotted grey lines show the impact of ignoring such a component. Even though a Kolgomorov-Smirnov test indicates only a 46% probability that the observed PNe luminosity distribution was drawn from the completeness-corrected theoretical form of the PNe luminosity function, here we still normalised the latter so that it would lead to an expected number of detected PNe that matches the one we observe (that is 12, including marginal detections).

4 RESULTS

In the context of understanding the connection between extragalactic PNe and the properties of their parent stellar population, we now consider the characteristics of the luminosity function of the PNe that we have identified in the central ∼20 arcsec of M31, which correspond to the inner ∼ 80 pc at the adopted distance of 791 kpc to this galaxy (i.e. $m - M = 24.49$ Tonry et al. 2001).

In particular, we wish to assess to what extent the central PNe of M31 could have been drawn from the generally adopted form of the PN luminosity function (PNLF) introduced by Ciardullo et al. (1989). This does not necessarily have to be the case given that central stellar populations of M31 are quite different, and in particular more metal-rich, than what is observed in the rest of this galaxy (which is where the PNLF form of Ciardullo et al. was mostly established) and than what is expected in the stellar halos of more distant galaxies where PNe are typically detected.

The central PNe luminosity function of M31 is presented in Fig. 8, where the F_{5007} values of Tab. 1 have been first converted into apparent V-band magnitudes following the $m_{5007} = -2.5\log F_{5007} - 13.74$ formula of Ciardullo et al. (1989) and then into absolute M_{5007} magnitudes using a distance modulus of 24.49 magnitudes. The solid line in Fig. 8 shows also the theoretical PNLF of Ciardullo et al., which needs to be corrected for the fact that progressively fainter PNe are harder to detect before testing whether such a PNLF model can be regarded as the parent distribution for the PNe that we observe. Still, we already note a possible lack of bright PNe in M31 compared to what would be expected from the standard form of the PNLF, which cannot be explained by this kind of limitation.

To compute the completeness function of our experiment, that is, the probability as a function of absolute magnitude M_{5007} that a PN of that brightness could be detected across the *entire* field-of-view of the SAURON observations for M31, we used a set of simulations similar to those performed in Paper I in the case of M32, even though here we also account for the adverse impact that the presence of diffuse ionised-gas emission has on the detection of PNe. These simulations, which are shown in Fig. 9 (see also the figure caption for details), illustrate how PNe of an absolute magnitude $M_{5007} \sim -1.0$ and fainter would quickly escape detection over most of the SAURON field-of-view, which is consistent with the fact that most of the detection limits for our PNe sources (shown with open diamonds in Fig. 8) pile up from a $M_{5007} \sim -1.5$ and above.

The completeness-corrected standard form for the PNLF is shown by the dashed line in Fig. 8, whereas the grey dashed line indicates the limit of our experiment if no diffuse ionised-gas emission were present in the nuclear regions of M31, which allows a comparison to our previous PNe survey in M32. In both cases, the dotted lines show the associated uncertainties on these functions. Accounting for incompleteness, a Kolgomorov-Smirnov test reveals that there is just a 46% probability that the observed PNe luminosity distribution was drawn from the theoretical prescription of Ciardullo et al., which is hardly surprising given the difference at the high-luminosity end between such a model and our data. In fact, a second set of simulations suggest that the apparent lack of bright PNe in our data could only result from a rather unfortunate sampling of the standard PNLF.

More specifically, starting from an intrinsic Ciardullo et al. shape of the PNLF and adopting a normalisation leading to match the number of observed PNe once the PNLF is corrected for incompletess (as is in fact the case for all the lines shown in Fig. 8), we generated a number of synthetic PN fields by considering at any particular position in the SAURON field of view the probability of having a PN of a given luminosity. Such a probability function simply corresponds to the total intrinsic PNLF rescaled by the fraction of stellar light that is observed in the SAURON spatial bin that is being considered. The [O III] flux of the simulated PNe was then “observed” by obtaining maps for the A/rN ratio and by applying the same detection criteria described in §3.2, including checking whether a synthetic PN would be detected against the known background of diffuse ionised-gas emission. Based on a thousand of such synthetic PNe fields, only in 8.5% of the cases we could not find any PN brighter than $M_{5007} = -3.0$, the current maximum PNe luminosity observed in the nuclear regions of M31.

This suggests that the standard form of the PNLF may not entirely apply to the nuclear regions of M31, and that the observed dearth of bright PNe in Fig. 8 may be real.

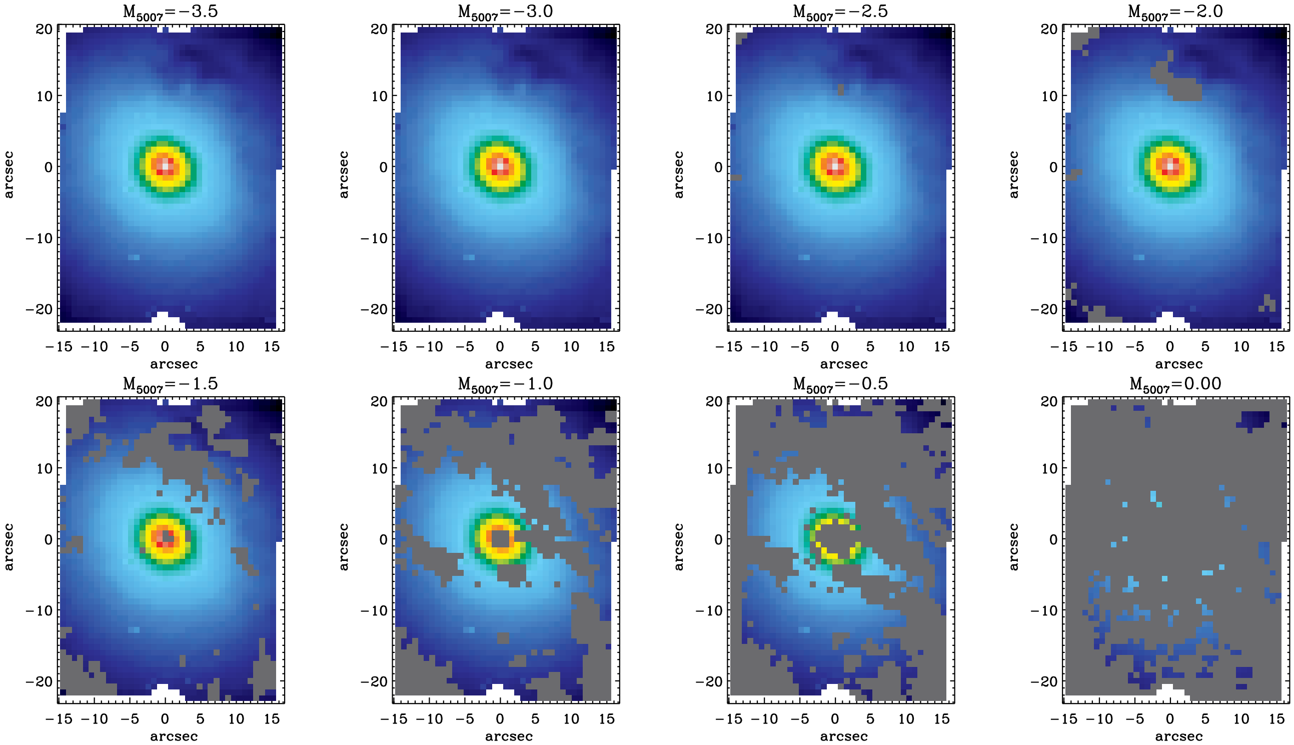

Figure 9. Reconstructed optical images of M31, in logarithmic flux scale, showing with grey bins the regions where, from left to right, PNe of decreasing luminosity would escape detection. To check whether in a given `SAURON` bin a PN of absolute magnitude M_{5007} would be detected, we generated at that position a Gaussian model for the [O III] flux of a PN of that brightness at the distance of M31, deriving also the corresponding spectral density values for the amplitude of the [O III] line. Using the values for the level of the noise rN in the residuals of our spectral fits we then computed the values of the A/rN ratio around the PN position and, using the criterion introduced in § 3.2, simply checked whether $A/rN > 4$ within a FWHM from the centre of the Gaussian model, which in these particular simulations correspond to the centre of the `SAURON` bins. Furthermore, in the presence of diffuse ionised-gas emission we also required that the peak [O III] flux for the simulated PNe exceeds by more than three times the diffuse nebular flux, where the latter was taken to be the background level estimated during our spatial fits (see Fig 5) in regions where a PN was actually found in our data. Since the number of PNe scales with the number of stars, at any M_{5007} value the ratio of the stellar flux observed where PNe of that absolute magnitude can be detected over the total stellar flux encompassed by our field-of-view corresponds the probability that a PN of that M_{5007} value could be detected during our observations, thus serving to construct our completness function. Uncertainties on such a function can be estimated by randomly placing the PNe Gaussian models within each `SAURON` $0.''8 \times 0.''8$ bin, rather than exactly at their centres.

5 DISCUSSION

The previous results on the luminosity function of the PNe found in the very central regions of M31 (within 80 pc) are at odds with the outcome of our earlier integral-field spectroscopic study of the PNe population in the optical regions of M32 (within one R_e). For that galaxy, the standard form of the PNLF could indeed be considered, to a fair degree of confidence, as the parent distribution of the PNe that we detected, with no significant features in their observed distribution function. We can attempt to interpret such a discrepancy by considering even the differences between the properties of the stellar populations encompassed by our `SAURON` observations for these two galaxies, in particular as regards the average value of their metallicity. A stronger stellar metallicity can indeed drive a larger mass-loss rate efficiency during the RGB phase, which in turn would reduce the number of HB stars with a massive H-shell that will eventually become bright PNe.

Even though there exist numerous stellar population studies in the literature on M31 and M32 (see, e.g., Saglia et al. 2010 and Rose et al. 2005, respectively) we can use our own `SAURON` data to compare the mean values for the stellar age and metallicity in these two galaxies in a more consistent way than possible when using different absorption line-strength measurements from the literature. For this, we co-added all the spectra in our data cubes after subtracting the emission from both PNe and diffuse ionised-gas components, and proceeded to fit such a total spectrum with the `pPXF` method of Cappellari & Emsellem (2004), using the entire MILES stellar library of Sánchez-Blázquez et al. (2006). We then combined the original stellar spectra from this library according to the relative weights that they were assigned during the `pPXF` fit, in order to obtain what effectively is the optimal stellar spectrum for representing the nuclear and central stellar populations of M31 and M32, respectively. Finally, we measured the strength of the standard Hβ, Fe5015 and Mgb indices from the Lick/IDS system on such optimal template, and followed Kuntschner et al. (2010) to compute from the Fe5015 and Mgb indices the more purely metallicity-sensitive [MgbFe50]' index, which is defined as $(0.69 \times \mathrm{Mg}b + \mathrm{Fe5015})/2$.

The use of the MILES optimal templates allows us to circumvent problems related to an imperfect sky subtraction and relative flux calibration on the `SAURON` data, while obtaining at the same time index values that are automatically corrected for kinematic broadening. Such an approach is recommended only if the templates can match almost perfectly the real data, which is generally the case when using such a large library as the MILES one, even

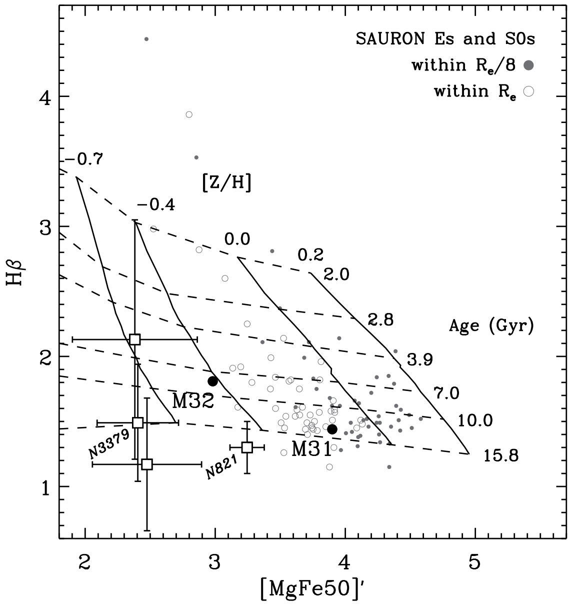

Figure 10. The Hβ vs [MgFe50'] diagnostic diagram of Kuntschner et al. (2010) where the stellar age and metallicity of the central 80 pc of M31 can be compared with i) that of the optical regions of M32 (i.e., within its effective radius R_e), ii) that of the 48 early-type galaxies of the `SAURON` sample (within both one R_e and $R_e/8$ as shown by the open and filled grey circles, respectively; from Kuntschner et al. 2006) and iii) with what found using the `SAURON` spectrograph in the halos of NGC 3379 and NGC 821 (open squares, from the measurements of Weijmans et al. 2009 centred between 3 and 4 R_e for NGC 3379 and at around one R_e for NGC 821). The age and metallicity grids are from the models of Schiavon (2007), as adapted for the study of Kuntschner et al. (2010). The central stellar population of the `SAURON` early-type galaxies tend to be more metal-rich than what is observed in the nuclear regions of M31, which on the other hand display a stellar metallicity value that generally exceeds what found within the whole optical regions of early-type galaxies. In fact, that would appear to be certainly the case of low-mass objects such as M32, which sports a value for the stellar metallicity within its optical regions that is more akin, although not as low, to what is observed in the halos of early-type galaxies.

when considering the spectra of massive early-type galaxies (e.g., Sarzi et al. 2010; Oh et al. 2011) where an overabundance of α elements usually poses a problem for a detailed spectral fitting (e.g., in the Mg*b* region).

Fig. 10 shows the relative location of M31 and M32 in the [MgFe50]' vs Hβ diagnostic diagram, where an estimate for the mean age and metallicity of their nuclear and central stellar populations, respectively, can be read through the model grids of Schiavon (2007). In Fig. 10 we also plot the values for the same indices for the early-type galaxies in the `SAURON` representative sample, measured within both one R_e and $R_e/8$ (data from Kuntschner et al. 2006), and for the stellar halos of NGC 821 (at a distance of one R_e) and NGC 3379 (at a distance between 3 and 4 R_e) from Weijmans et al. (2009).

The `SAURON` data confirm that the central 80 pc of M31 are more metal rich than the stellar population found in the central regions of M32, consistent with the hypothesis whereby an enhanced stellar-mass loss in the RGB that is driven by a larger metallicity would eventually lead to the observed lack of bright PNe in M31. In fact, our PNe findings appear to be independently backed up by Rosenfield et al. (2012) who, thanks to *HST* observations, finds that the relative number of bright post-AGB stars to that of fainter early post-AGB or AGB-manqué stars steadily decreases towards the centre of M31, nicely following also the central metallicity gradient measured by Saglia et al. (2010). These results would indeed agree with a dimming of the PNLF given that only post-AGB stars can power the brightest PNe, while supporting also the idea that a larger stellar metallicity is responsible for it. As regards M32, on the other hand, Fig. 10 shows that the optical regions of this galaxy have a value for the stellar metallicity that is close, though not as low, to what Weijmans et al. (2009) estimated with `SAURON` data in the halos of the early-type galaxies NGC 3379 and NGC 821. Since also the measurements of Weijmans et al. (2009) are based on `SAURON` data, all the values shown in Fig. 10 can be consistently compared to each other. If metallicity is indeed related to the lack of post-AGB stars and bright PNe in the nuclear regions of M31, then such a similarity may help understand why the central PNe population of M32 appears on the contrary to be consistent with the Ciardullo et al.'s form for the PNLF as in the case of the peripheral PNe populations of galaxies.

Rosenfield et al. also show that the central metallicity gradient of M31 corresponds closely to an increase in the far-UV excess towards the centre of M31, much as observed when these quantities are measured in different objects at larger galactic scales (Burstein et al. 1988; Bureau et al. 2011; Jeong et al. 2012) and consistent with the presence of a large number of AGB-manqué stars. This contrasts again with the case of M32, which has long been known to display little or no far-UV excess flux (Burstein et al. 1988).

Finally, we note that in terms of their stellar metallicity the nuclear regions of M31 fall roughly in between what is observed in the central metal-rich stellar populations of early-type galaxies (within $R_e/8$) and what is found on average within the effective radius R_e of these objects (Fig 10, according always to measurements based on `SAURON` data). This suggests that also the PNe population of the optical regions of early-type galaxies could display a similar dearth of bright PNe as found in the central 80 pc of M31, which is a possibility that could have a significant impact on the presently rather loose anti-correlations between the specific number of PNe and either the stellar metallicity or the strength of the UV-upturn (Buzzoni, Arnaboldi, & Corradi 2006; Coccato et al. 2009). In fact, it may be even possible that the current trends reflect a decrease only in the number of bright PNe in the halo of early-type galaxies with progressively larger central (and presumably also peripheral) metallicity values, rather than a change in the overall specific content of PNe. This may not be too far fatched considering that the completeness limit of most PNe surveys in external galaxies does not extend beyond 1 to 2.5 magnitudes from the peak PN magnitude of $M_{5007} = -4.47$ (see, e.g., Tab. 5 in Buzzoni, Arnaboldi, & Corradi 2006) so that we only have a limited view on the shape of the PNLF of galactic halos.

6 CONCLUSIONS

Building on our previous integral-field spectroscopic study for the central PNe population of M32, in this paper we have further investigated the very central ∼80 pc of M31 and found that:

- integral-field spectroscopy allows to detect PNe also in the presence of emission from diffuse gas, as commonly observed in early-type galaxies and in the bulge of spirals.
- our relative inexpensive `SAURON` data could spot nearly all the PNe found in *HST* narrow-band band images, measuring total

[O III]$\lambda 5007$ flux values well in agrement with the *HST* measurements.

- contrary to the case of the central regions of M32, the nuclear PNe population of M31 is only marginally consistent with the generally adopted Ciardullo et al. form of the PNe luminosity function
- such a discrepancy is due to an observed lack of PNe with absolute magnitude M_{5007} brighter than -3.0, which simulations suggest would occur only considering a rather unfortunate (in 8.5% of the cases) sampling of such a model PNLF.

Considering that the nuclear stellar population of M31 is characterised by a larger stellar metallicity and a much stronger far-UV excess compared to what is found in the central (within one effective radius) regions of M32, the previous results would appear to support the idea that a larger metallicity (which enhances the stellar-mass loss efficiency in the RGB) can lead to an horizontal-branch population that is more tilted toward less massive and hotter He-burning stars, so that its progeny consists mostly of UV-bright AGB-manqué stars, but few, if any, bright PNe.

A lack of bright PNe is also consistent with the recent reports by Rosenfield et al. (2012) on a shortage of post-AGB stars towards the nucleus of M31, since bright PNe are powered by central post-AGB stars. If such a dearth of post-AGB stars and bright PNe does indeed correspond to nearly-solar values for the stellar metallicity or above, then such a feature is likely to characterise also the PNe luminosity function in the optical regions of more distant and massive old stellar systems, which would imply that the PNLF form of Ciardullo et al. (1989) is not universally applicable. This is in fact a possibility that will be explored in future papers that will use the `SAURON` data already at hand for the complete ATLAS^{3D} sample of early-type galaxies (Cappellari et al. 2011), circumnventing the need for a prohibitively expensive narrow-band imaging campaign with *HST*.

ACKNOWLEDGEMENTS

We are grateful to Laura Greggio, Alvio Renzini, Enrico Maria Corsini, and Harald Kuntschner for their suggestions. We also thank the referee Michael G. Richer for providing very useful comments that improved the quality of this manuscript. NP acknowledges the University of Hertfordshire for funding his visit at the Centre for Astrophysics research where most of this study was carried out. NP and MS are also grateful, respectively, to the Astronomy Department of the University of Padova and to the European Southern Observatory for their hospitality. Finally, MS and MC acknowledge their respective STFC Advanced (ST/F009186/1) and Royal Society University Research fellowships.

REFERENCES

Bacon R., et al., 2001, MNRAS, 326, 23
Bacon R., Emsellem E., Combes F., Copin Y., Monnet G., Martin P., 2001, A&A, 371, 409
Bacon R., et al., 2006, The Messenger, 124, 5
Brown T. M., Smith E., Ferguson H. C., Sweigart A. V., Kimble R. A., Bowers C. W., 2008, ApJ, 682, 319
Bureau, M., Jeong, H., Yi, S. K., et al. 2011, MNRAS, 414, 1887
Burstein, D., Bertola, F, Buson, L. M., Faber, S. M., Lauer, T. R., 1988, ApJ, 328, 440
Buzzoni A., Arnaboldi M., Corradi R. L. M., 2006, MNRAS, 368, 877
Cappellari M., Copin Y., 2003, MNRAS, 342, 345
Cappellari M., Emsellem E., 2004, PASP, 116, 138
Cappellari M., et al., 2011, MNRAS, 413, 813
Ciardullo R., Jacoby G. H., Ford H. C., Neill J. D., 1989, ApJ, 339, 53
Ciardullo R., Durrell P. R., Laychak M. B., Herrmann K. A., Moody K., Jacoby G. H., Feldmeier J. J., 2004, ApJ, 614, 167
Ciardullo R., Sigurdsson S., Feldmeier J. J., Jacoby G. H., 2005, ApJ, 629, 499
Ciardullo R., 2006, IAUS, 234, 325
Coccato L., et al., 2009, MNRAS, 394, 1249
de Zeeuw P. T., et al., 2002, MNRAS, 329, 513
Douglas N. G., et al., 2007, ApJ, 664, 257
Dopita M. A., et al., 1997, ApJ, 474, 188
Emsellem, E., et al. 2004, MNRAS, 352, 721
Falcón-Barroso J., et al. 2006, MNRAS, 369, 529
Greggio L., Renzini A., 1990, ApJ, 364, 35
Greggio L., Renzini A., 1999, MmSAI, 70, 691
Jacoby G. H., Ciardullo R., Ford H. C., 1990, ApJ, 356, 332
Jacoby G. H., et al., 1992, PASP, 104, 599
Jacoby G. H., Ciardullo R., 1999, ApJ, 515, 169
Jeong, H., Yi, S. K., Bureau, M., et al. 2012, MNRAS, 423, 1921
Kuntschner H., et al., 2006, MNRAS, 369, 497
Kuntschner H., et al., 2010, MNRAS, 408, 97
Mamon G. A., Dekel A., Stoehr F., 2005, AIPC, 804, 345
Marigo P., Girardi L., Weiss A., Groenewegen M. A. T., Chiosi C., 2004, A&A, 423, 995
Merrett H. R., et al., 2006, MNRAS, 369, 120
Oh K., Sarzi M., Schawinski K., Yi S. K., 2011, ApJS, 195, 13
Richer M. G., Stasińka G., McCall M. L. M., 1999, A&AS, 135, 205
Romanowsky A. J., Douglas N. G., Arnaboldi M., Kuijken K., Merrifield M. R., Napolitano N. R., Capaccioli M., Freeman K. C., 2003, Sci, 301, 1696
Rosenfield P., et al., 2012, ApJ, 755, 131
Rose J. A., Arimoto N., Caldwell N., Schiavon R. P., Vazdekis A., Yamada Y., 2005, AJ, 129, 712
Saglia R. P., et al., 2010, A&A, 509, A61
Sánchez-Blázquez P., et al., 2006, MNRAS, 371, 703
Sarzi M., et al., 2006, MNRAS, 366, 1151
Sarzi M., et al., 2010, MNRAS, 402, 2187
Sarzi M., Mamon G. A., Cappellari M., Emsellem E., Bacon R., Davies R. L., de Zeeuw P. T., 2011, MNRAS, 415, 2832 (Paper I)
Schiavon R. P., 2007, ApJS, 171, 146
Tonry J. L., Dressler A., Blakeslee J. P., Ajhar E. A., Fletcher A. B., Luppino G. A., Metzger M. R., Moore C. B., 2001, ApJ, 546, 681
Weijmans A.-M., et al., 2009, MNRAS, 398, 561